International Journal of Engineering Innovation & Research
Volume 7, Issue 1, ISSN: 2277 – 5668

Numerical and Experimental Study of Evaporation of Liquid Effluent Flowing on an Inclined Plate

H. ZOUAGHI[1,2*], S. BEN JABRALLAH[2,3] and S. HARMAND[4]
[1]National Engineering School of Monastir, Avenue Ibn El Jazzar, 5019, Monastir, Tunisia.
[2]Laboratory LETTM, Sciences Faculty of Tunis, University Campus, 2092, Tunis El Manar, Tunisia.
[3]Sciences Faculty of Bizerte, Zarzouna, 7021 Bizerte - Tunisia.
[4]University of Lille Nord, UVHC – LAMIH UMR CNRS 8201, Mont Houy, Valenciennes, Cedex 09, 59300, France.
*Corresponding author email id: hibazouaghi@yahoo.fr

Date of publication (dd/mm/yyyy): 08/02/2018

***Abstract* – This work deals with the recovery of liquid effluent by thermal evaporation. The effluent is a digestate of pig manure which is subjected to anaerobic digestion and phase separation by centrifugation. Its dry matter is about 2.3%. The goal is to minimize its water content and to use it as a fertilizer on agricultural soils.**

The evaporator consists on a stainless steel plate inclined by 30°. The plate is exposed to solar simulator radiations which heat flux is about 452W/m² in average. Once plate temperature is stabilized, the liquid is injected from the top of the plate.

The cartography of the plate temperature is obtained by two methods; the first is measured and the second is made by calculating from thermal balances.

Evaporation tests were performed. The device is, on one hand, covered with a glass, and removed, on the other hand. A comparison between measured evaporated mass flow and calculated from mass balances is determined in laminar regime. It depends on many parameters, especially on heat flux, air, plate and liquid temperature.

***Keywords* – Evaporation, Effluent, Balance, Heat Flux, Mass Flow.**

I. INTRODUCTION

Evaporation needs heat that can provide from the sun, reducing the use of fossil energy. Many studies were performed in such solar energy applications as desalination, distillation ([1], [2], [3] and [4]) and drying ([5] and [6]).

Mezzache *et al.,* [7] worked on the effects of inlet conditions on evaporation processes. They studied the effect of inclination and improves that when the temperature of the wall or heat flux are fixed, mass flow rate and gas velocity are strongly related to the inclination. When the angle is between 0 and 10°, evaporated flow rate increases with the increase of the angle of inclination. The inclination has also an impact on heat and mass transfer and on lower velocity of the gas. Their work indicates that when the inclination angle is near 10°, its effect reaches its maximum.

Thiele *et al.,* Jingchun *et al.,* and El Agouz *et al.,* studied different solar systems and its effects on evaporation. Thiele *et al.,* [2] worked on the behavior of a thin liquid film on a uniformly heated smooth solid substrate is considered. They found that when the substrate is horizontal and the Marangoni number sufficiently large the film breaks up into a periodic array of drops. When the substrate is slightly inclined this drop-like state slides down the substrate. El Agouz *et al.,* [4] focus their work on the rating of the performance of a solar desalination device. The system is an inclined continuous water flow. They studied the effect of the thickness and velocity of the film flowing on the plate and air wind velocity. They tested those parameters on three models.

The first model consists on an inclined solar still with a continuous injection of water on an open circuit. However, the second one is the same inclined solar still but with closed circuit without water makeup. The third one is like the second one but with a water makeup.

Testing the effects of different parameters on the three models, they found that the solar still of the third model has the best productivity of 57,2% than the two other models. The first model is only recommended when it's combined with other desalination system because of high temperature at the outlet. The best improvement corresponds to the third model; the first one has the lowest performance. They conclude that to improve the still system productivity and efficiency, it's important to optimize film thickness, water velocity and wind velocity.

The same principle is studied by Aybar *et al.,* [1], Aybar [8] and Agboola *et al.,* [9]. The aim is to ameliorate the behavior of the solar still system by varying its different operating parameters. El-Agouz [10] presented experimentally performance of stepped solar still when water circulates continuously. He sets up a tank to storage see and salt water. The goal is to have a better productivity. The daily efficiency found was better than for the conventional still. It is approximately about 20%

Jingchun *et al.,* [3] established a theoretical analysis of water film evaporation on an adiabatic wall. They found that the temperature of water surface falls as function of time. It continues its decrease until reaching the temperature of the air wet-bulb. Latent heat required for water is not only from heat conduction of film water at the first storage but also from convection between air and fluid when water temperature reaches air wet-bulb temperature.

Raimundo *et al.,* [11] numerically simulated water film evaporation in airstream and discussed the effects of air velocity, water and air temperature and air relative humidity on the evaporation rate. Yang *et al.,* [12] and Yu *et al.,* [13] studied water film evaporation on solid surfaces using molecular dynamics simulation method. Leu *et al.,* [14] experimentally investigated water film evaporation on a vertical plate having a thin porous layer as a cover. This layer improves heat and mass transfer during evaporation process.

In this paper, solar system is used for drying liquid effluent. The purpose is to reduce pollution caused by this waste and to recover it as a fertilizer for agriculture soils.

This study is about evaporation of liquid effluent on a stainless steel plate inclined of 30°. The effluent consists on the liquid phase of a pig digestate passed by phase separation by centrifugation. Its water content is about 97,7%. The evaporator used in this work has 2m long and 1m wide. A solar simulator is used for evaporation. Its power is about 6000W. Two cases are studies. The stainless steel is, in the first case, directly exposed to solar simulator radiations. In the second case, the plate is covered with a glass which thickness is about 6mm.

The liquid effluent is injected from the top of the plate using a pump. A comparison between measured evaporated mass flow and calculated from mass balances is determined in laminar regime. It depends on heat flux, air, plate and liquid temperature.

II. Effluent Characteristics

Thermal conductivity "λ" heat capacity "Cp" and dynamic viscosity "μ" of the liquid effluent were determinate in the case of thermo-physical characterization. The effluent presents the liquid phase of pig manure previously recovered using methanation process and a separation phase by centrifugation.

Thermo-physical characterization is made on three samples (E_0, E_1 and E_2) which concentrations are respectively (C_0, C_1 and C_2). The concentration C_0 corresponds to the sample E_0 having a density of 960g/l and a dry matter content of 2.3%. The sample E_1 is prepared from the sample E_0. Evaporating the sample E_0 and losing the third of its initial volume, we obtain the sample E_1 which concentration is C_1 and a density of 900g/l. By preparing the sample E_2, we have to evaporate 2/3 of the volume of E_0. Sample characteristics are presented in Table 1.

Table 1: Characteristics of the different samples

Sample	E_0	E_1	E_2
Concentration	C_0	$C_1=1.5C_0$	$C_2=3C_0$
Density (g/l)	960	900	850

The FP2C is a thermal conductivity meter used to determine thermal conductivity. The measurement principle follows the hot wire method for measuring the total thermal conductivity of the material from changes in temperature. This temperature is measured using a thermocouple placed close to a resistive wire.

Thermal conductivity is called "λ" which values are expressed in W/m.K. Measurements accuracy is about 5% and samples temperature is between 30 and 60°C as presented in Table 2.

Table 2: Samples thermal conductivity (W/m.k)

Sample	E_0	E_1	E_2	Water
T = 30°C	0.593	0.560	0.598	0598
T = 60°C	0.700	0.805	0.713	0.651

It's seen that thermal conductivity doesn't depend on samples concentrations; it depends on its temperature. Thermal conductivity is about 0.584 W/m.K when sample is heated at 30°C comparing to water which thermal conductivity is about 0.598W/m.K for the same temperature. When sample temperature is about 60°C, its thermal conductivity is about 0.739W/m.K, comparing to water thermal conductivity which is about 0.651W/m.K [15].

Dynamic viscosity is measured using a rheometer DHR III which mark is TA Instrument. Dynamic viscosity measurements are conducted for three temperatures which are 20, 45 and 70°C at atmospheric pressure. In order to assess the reproducibility, each test was repeated twice.

The first step consists on deposing sample on bottom plate and diffusing with the top plate. Using a spatula, we remove excess product and then we can start tests. The accuracy of temperature measurement is about 0.5°C.

Using a measuring method which consists on a constant shear rate, dynamic viscosity curves are obtained. The viscosity and share stress are presented at the same moment than the flow is occurred. Taking account of geometric imperfections and device accuracy, measurements have an accuracy of 10%. The variation of dynamic viscosity as function of temperature is presented in fig.1.

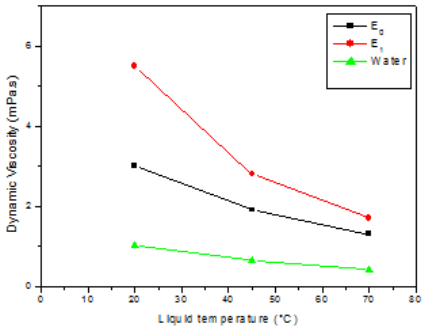

Fig. 1. Dynamic viscosity for samples E_0 and E_1

It's seen that for the two samples, dynamic viscosity is influenced by temperature. Dynamic viscosity decreases with the increase of temperature. The influence of temperature is well seen for E_0 and E_1 when temperature is between 20 and 45°C. As E_0 has the lowest concentration, its dynamic viscosity is closer to that of water [15].

The DSC Mettler Toledo DSC1 is the measurement apparatus used to determine the heat capacity of the sample E_0. Measurement principle consists on differential scanning calorimetry (DSC) method. Using a standard sapphire, it allows determining the variation in enthalpy.

To determine heat capacity, some experimental conditions have to be done. First, we have to stabilize temperature at 20°C during 5min. Then, heating can begin from 20 to 70°C using an increase of 20°C per minute. Once temperature is at 70°C, we have to stabilize it during 5min. Next, a regular scan has done for neutral gas of nitrogen until 50ml/min. The variation of heat capacity of the sample E_0 comparing to water is presented in fig. 2.

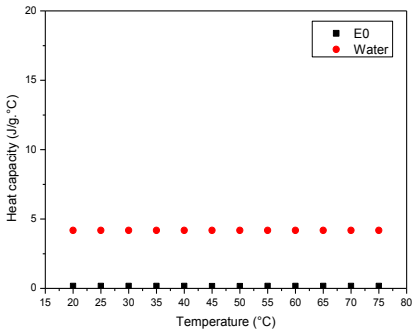

Fig. 2. Variation of heat capacity function of temperature

From fig.2, it's seen that for sample E_0, heat capacity still constant for a temperature varying between 20 and 75°C. At this temperature range, heat capacity is about 0.166 J/g.°C in average comparing to water which heat capacity is about 4.182 J/g.°C in average.

III. Experimental Device

This process consists on flowing the aqueous liquid effluent on a stainless steel plate exposed to solar simulator radiations. In order to recover liquid waste like digestate which is rich in nutriment, we choose to evaporate. The final product will be used in agricultural soils as fertilizer. The system should be inexpensive and consume as little energy as possible to enable widespread adoption of the system by farmers who make methane.

This device is an evaporator composed of stainless steel plate inclined of 30°. The plate has those dimensions (2m×1m). Tests have done firstly when the plate is directly exposed to solar radiations. Then, it will be covered with a laminating glass which thickness is about 6mm. The glass cover is resistant to high temperature above 80°C. Using nozzle and a pump that feeds dispense manifold, the effluent is injected from the top of the inclined plate. It's at steady state when plate temperature is stabilized, that the liquid is injected. After circulating on the plate, the liquid is collected in the gutter. The experimental device is schematized in Fig. 3.a.

The steel plate is insulated on the underside with glass wool. The steel plate is heated using a 6000W solar simulator. The solar simulator is placed parallel to the plate at a distance of 2m, such that heat flux will be similar to solar heat flux in average.

To measure plate temperature, many thermocouples are fixed in three columns of nine lines as presented in Fig. 3.b. The thermocouple positioned at X_1=0.15m and Y_1=0.25m. The distance between thermocouples is about 0.325m in abscissa X and 0.20m in ordinate Y.

In this devise, thermocouples used are a K-type having a margin of error of ± 0.5°C.

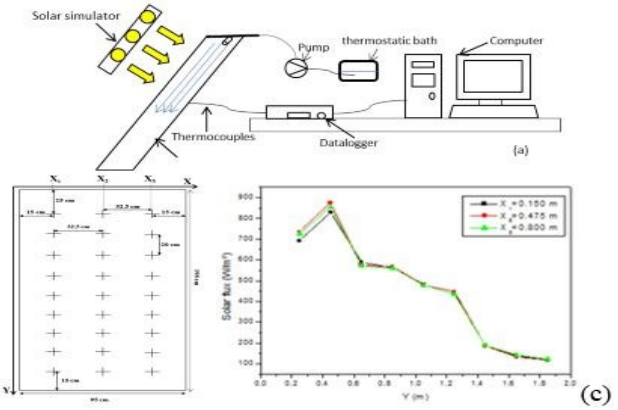

Fig. 3. (a) Schematic diagram of the evaporator; (b) layout of thermocouples on the plate; (c) cartography of heat flux

Weighing the effluent before and after injecting the liquid without solar simulator radiation, we can determine the values of the inlet mass flow. After liquid injection and the stabilization of the plate temperature, evaporated flow rate is determined by weighing the liquid at the outlet and remove the value of the inlet flow rate, during a determined time.

Results will be compared when the plate is directly exposed to solar radiation and when it's covered with a glass cover.

The cartography of the flux is shown in Fig. 3.c. We chose the same points as the thermocouples (three columns of nine lines). The solar flux is measured using a pyranometer with accuracy ±4µV/W/m².

The maximum flux is at Y=0.45m, according to the different positions X_1, X_2 and X_3. The flux is 874W/m² at Y=0.45m for position X_2. The minimum flux is 116W/m² at Y=1.85m for position X_1. The mean flux along the plate is approximately 452W/m².

The temperature profile of the steel plate in steady state has the same shape than heat flux. Its maximum is about 75°C. Because the heat flux of solar simulator is focused on the second column, the temperatures are the greatest at that column. When x=45cm, the plate temperature is greater.

At steady state, the maximum temperature of the glass is approximately 40°C.

IV. Numerical Scheme

Firstly, the plate is exposed the solar simulator radiations. The heat balances on the plate and glass will be determined before the injection of the liquid and after the stabilization of plate temperature.

IV.1. *Plate without glass cover*

The back of the plate is well isolated. Supposing that there are no heat losses, heat balance on the plate is determined based on the sum of the incoming flux equals the amount of outgoing flux [16].

$$\alpha_p I_0 - \varepsilon_p \sigma\left(T_p^4 - T_{air}^4\right) - h_{ext,pa}\left(T_p - T_{air}\right) = 0 \qquad (1)$$

In steady state, the natural convection coefficient is function of plate and air temperature. According to [17] and [18], it can be written:

$$h_{ext,pa} = \frac{5}{4}\left[\frac{\mathrm{Pr}}{4+9\sqrt{\mathrm{Pr}}+10\mathrm{Pr}}\right]^{2/5}\left(\mathrm{Pr}\times\frac{\beta l^3}{\upsilon^2}\times\sin a\right)^{1/5}(T_p - T_{air})^{1/5} \quad (2)$$

So, heat balance takes this form:

$$\alpha_p I_0 - \varepsilon_p\sigma\left(T_p^4 - T_{air}^4\right) - 0.225\left(T_p - T_{air}\right)^{5/4} = 0 \quad (3)$$

The effluent is now injected from the top on the plate because its temperature stabilized. Heat balance on the film is schematized in fig.4.

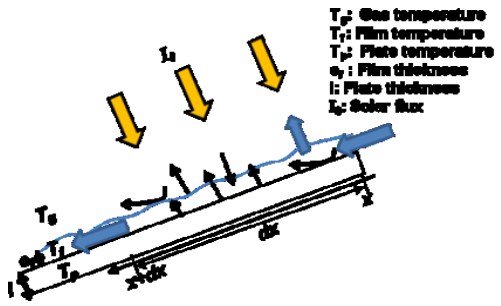

Fig. 4. Scheme of liquid film balance

From fig.4, film heat balance takes this form, knowing that the sum of the incoming flux equals the amount of outgoing flux:

$$\alpha_p\tau_f I_0 + \varepsilon_p\alpha_p\sigma T_f^4 - \varepsilon_p\sigma T_p^4 - h_{\mathrm{int},pf}\left(T_p - T_f\right) = 0 \quad (4)$$

In steady state, the forced convection coefficient between the liquid effluent and the plate is inversely proportional to film thickness. It depends on the inlet flow, viscosity and thermal conductivity of the effluent [19].

$$h_{\mathrm{int},pf} = \left(0.332.\frac{\lambda}{L}\mathrm{Pr}^{1/3}\sqrt{\frac{m_{in}}{\upsilon}}\right)\frac{1}{\sqrt{e_f}} \quad (5)$$

The mass balance can be determined as [20], [21] and [23]:

$$\dot{m}(x)Cp\frac{T_f(x)}{dx} + \alpha_f I_0 + \alpha_f\tau_f\rho_p I_0 + h_{\mathrm{int},pf}\left(T_p(x) - T_f(x)\right) + \alpha_p\varepsilon_p\sigma T_p^4$$
$$= \left(\dot{m}(x) - \dot{m}(x+dx)\right)Lv + h_{\mathrm{int},fair}\left(T_f - T_{air}\right) + \varepsilon_f\sigma T_f^4 + \dot{m}(x+dx)Cp\frac{T_f(x+dx)}{dx} \quad (6)$$

Where: $S_p = dx.L$ and $\dot{m}_{ev} = \dot{m}_{in} - \dot{m}_{out}$ (7)

The film thickness along the plate is variable; it depends on the evaporated flow. Assuming the volume is constant, an approximation is determined; it allows defining the film thickness and volume concentration by:

$$e_f(x) = e_f(0).\frac{m(x)}{m_{in}} \quad \text{with} \quad m(x) = m_{in} - \sum m_{ev}(x) \quad (8)$$

$$Cv(x) = Cv(0)\frac{e_f(0)}{e_f(x)} \quad (9)$$

Knowing that the number of unknowns is bigger than the number of equations, the mass and heat balances are solved one by one. The software used to solve equations is MATLAB. Firstly, and before film circulating, plate temperature is determined from (3). After the injection of the liquid and the stabilization of plate temperature, those data are directly entered in (4). The convection coefficient is then calculated.

Therefore, (6) can be solved at initial status knowing the initial, film temperature and thickness. The initial film thickness is determined from (8) and the same approach is used to solve (5) and (6).

IV.2. *Plate with a glass cover*

Based on the sum of the incoming flux equals the amount of outgoing flux, the heat balance on the glass cover can then be written ([20] and [23])

$$S_v\alpha_v I_0 + S_v\alpha_v\tau_v\rho_p I_0 + \varepsilon_v\varepsilon_p S_p\sigma T_p^4 - \varepsilon_v\sigma S_v T_v^4 + h_{ext}S_p\left(T_v - T_{air}\right) - h_{\mathrm{int}}S_p\left(T_v - T_g\right) = 0 \quad (10)$$

Heat balance on the plate before liquid circulating is [24]:

$$S_p\alpha_v\tau_v\rho_p I_0 + S_p\alpha_p\varepsilon_v\sigma T_v^4 - \varepsilon_p\sigma S_v T_p^4 - h_{\mathrm{int},pg}S_p\left(T_p - T_g\right) = 0 \quad (11)$$

Once plate temperature stabilized and the liquid circulates, heat balances on the plate and the glass cover become ([24], [25] and [20]):

$$S_v\alpha_v I_0 + S_v\alpha_v\tau_v\rho_f I_0 + \varepsilon_v\varepsilon_f S_p\sigma T_f^4 - \varepsilon_v\sigma S_v T_v^4 + h_{ext}S_p\left(T_v - T_{air}\right) - h_{\mathrm{int}}S_p\left(T_v - T_g\right) = 0 \quad (12)$$

$$\alpha_p S_p\tau_f\tau_v I_0 + \varepsilon_f\alpha_p\sigma S_p T_f^4 - \varepsilon_p\sigma S_p T_p^4 - h_{\mathrm{int},pf}S_p\left(T_p - T_f\right) = 0 \quad (13)$$

The mass balance takes this form ([20] and [21])

$$\dot{m}_{in}C_p\frac{T_f(x)}{dx} + \alpha_f I_0 + \alpha_f\tau_f\rho_p I_0 + h_{\mathrm{int},pf}\left(T_p(x) - T_f(x)\right) + \alpha_p\varepsilon_p\sigma T_p^4 = \dot{m}_{ev}L_v + h_{\mathrm{int},fg}\left(T_f - T_g\right) + \varepsilon_f\sigma T_f^4 + \dot{m}_{out}C_p\frac{T_f(x+dx)}{dx} \quad (14)$$

The convection coefficients and the resolution of balances equations are determined with the same method than VI.1.

V. Results and Discussion

A comparison between calculated results when the plate is covered with glass and without glass is made.

From fig.5, it's seen that the liquid temperature increases and decreases in the bottom of the plate. This shape can be explained by the distribution of heat flux on the plate which is maximum on the top of the plate; it decreases until stabilizing in the bottom of the plate.

By solving (4) and (12) we were able to compare temperature of liquid film in different positions in the two cases (case 1: covered with glass; case 2: plate with glass cover). Results are shown in fig. 5.

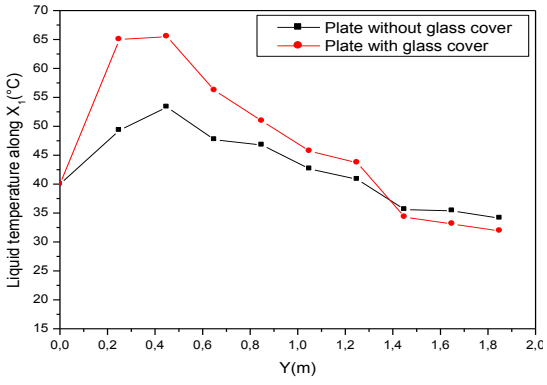

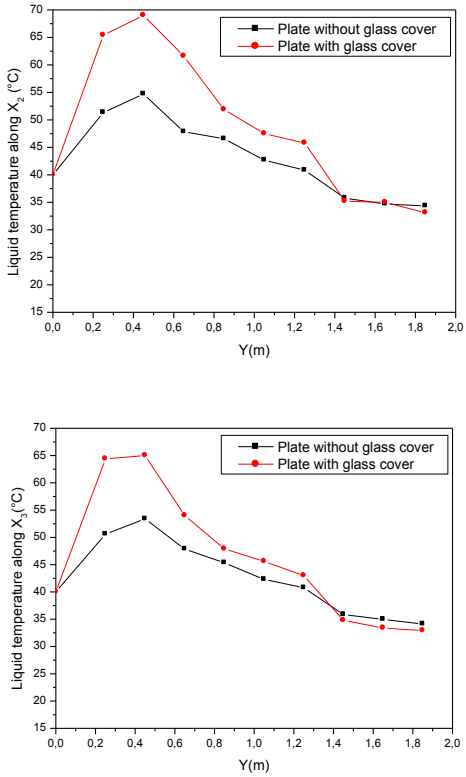

Fig. 5. Evolution of temperature of the liquid (preheated at 40°C) along the plate

Three curves have the same shape which is related to heat flux distribution. Results indicate that the fluid temperature is higher when the plate has a glass cover.

Liquid temperature increases on top of plate. Once the maximum of 69°C is reached at Y=0.45m and X_2=0.475m, liquid temperature begins decreasing to 33°C for Y=1.85m until it become constant at plate bottom. The maximum is attained at the column X_2 when the plate has a glass cover and for an inlet temperature of liquid is about 40°C. The shape of curves is strongly related to the distribution of the heat flux. By solving heat balances, it's seen that the variation of liquid temperature T_f depends on the variation of plate temperature Tp. Thus, the last one is related to heat flux repartition. This explains that liquid temperature and plate temperature have the same appearance.

Plate temperature is higher than liquid temperature in the top of the plate. In this part, plate heats the liquid film by convection process. That's why film temperature increases. However, when the liquid is approaching the bottom, it cooled because the plate isn't well heated. So, the fall of liquid temperature can be explained at the outlet.

Plate temperature is presented in fig.6 for an inlet liquid temperature of 40°C. It comes from the resolution of heat balances of (3) and (11).

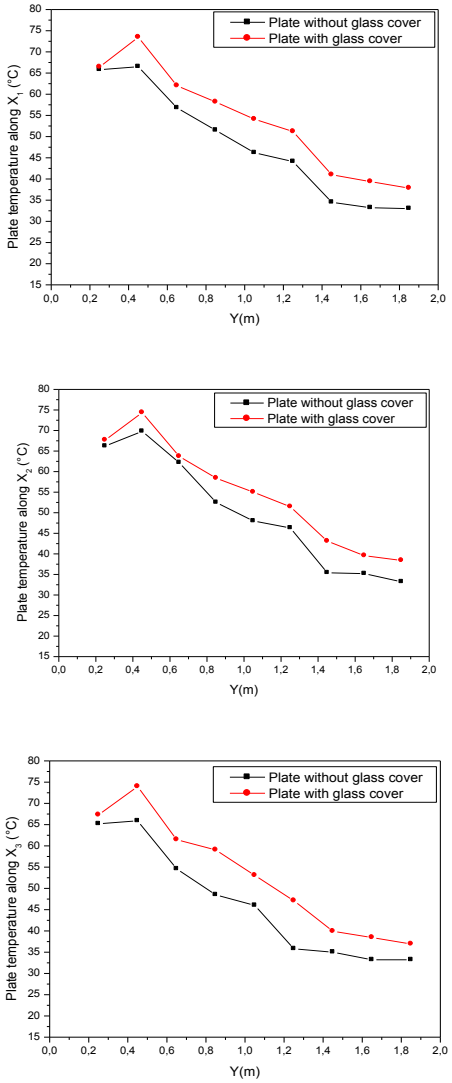

Fig. 6. Comparison between plate temperatures after liquid film circulating

Curves representing plate temperature following X_1, X_2 and X_3 have the same shape. It increases until attaining the maximum at Y=0.45m, then it decreases and stabilize at the bottom of plate. The maximum plate temperature corresponds to a maximum heat flux of 874W/m².

From heat balance, it's seen that plate temperature is strongly related to heat flux. So, when heat flux is maximum, plate temperature is maximum and inversely. As plate temperature falls because of the low heat flux in the part.

The difference between experimental and calculated results may depend on many parameters such as ambient temperature and the variation of the temperature of the air between plate and solar simulator.

The variation of evaporated flow rate per unit width is presented in fig.7. It's seen that it has the same shape that film temperature. It's maximum when film temperature is maximum. It gradually decreases. It is low in the bottom of plate because fluid temperature is low. Evaporated flow rate per unit width is better when the plate is covered. It's maximum about 0.032l/s.m along X_2.

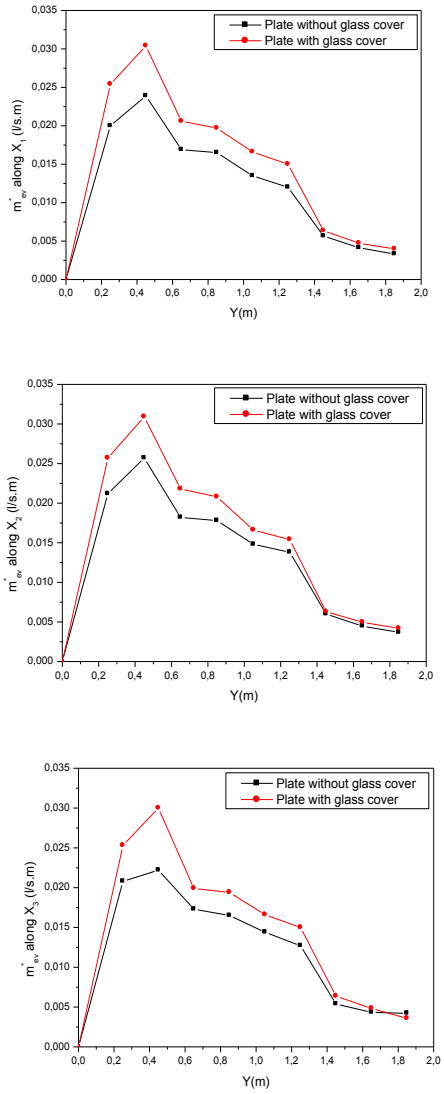

Fig. 7: Evaporated mass flow per unit width

Ben Jabrallah *et al.,* [26] worked on evaporation of falling film in distillation cell. The cell has a parallelepiped form with vertical walls. They studied heat and mass transfer in the cell. Studying the influence of heat flux density on distillate flow rate on the top and bottom of cell, they improve that for a constant inlet flow rate and temperature, evaporated flow rate increases with the increase of heat flux density.

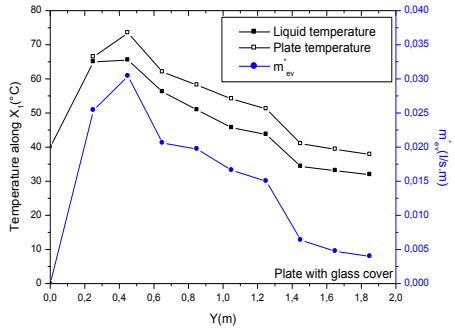

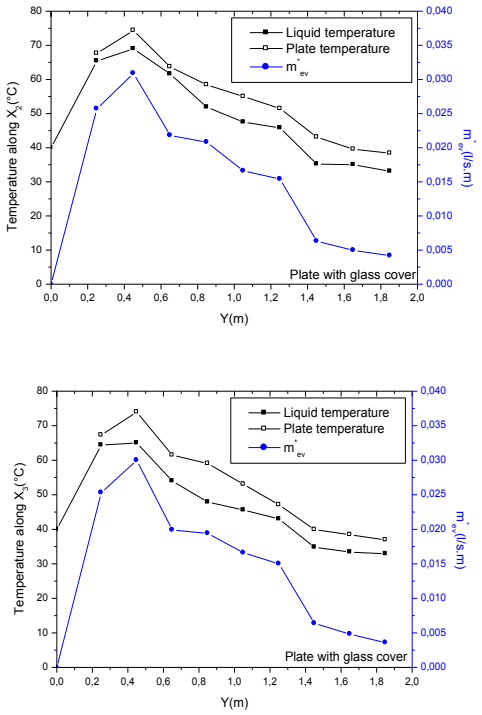

Fig. 8. Liquid and plate temperature and evaporated flow rate (plate with glass cover)

Liquid and plate temperature and evaporated flow rate per unit width have the same shape (fig.8). It indicates that the variation of evaporated flow rate is strongly related to the variation of liquid and plate temperature. This can be explained in numerical model by solving eq.10 to eq.14 when the plate is covered with glass.

The film thickness decreases along plate. By solving (8), film thickness depends on evaporated flow rate. When evaporated flow is maximum, film thickness is minimum. Since, evaporated flow is higher for X_2; the film thickness is lower in the two cases. In the bottom of the plate, evaporated flow rate is low, film thickness still constant in this part.

When the plate is covered with glass, film thickness is lower than when the glass is removed. This is due to evaporated flow rate which is maximum is this case. It's minimum for X_2.

Jingchun *et al.* [3] worked on one dimensional water film evaporation process. The theoretical model is composed of a water film attached to an adiabatic solid wall, with its other surface exposed to moist air. It has an initial temperature of T_0 and an initial thickness of δ_0. The moist air has a temperature of T_0 and a relative humidity of Φ_0 which is less than unity. They found that the variation of water film thickness with time can be expressed as: $\delta = \delta_0 - \frac{1}{\rho}\int_0^\tau J d\tau$.

ρ is the density of water and J presents water evaporation rate. They found that the variation of film thickness during the time isn't linear for different convective heat transfer coefficients and for $\delta_0 = 0.5mm$. Using the same equation in our model, results are in the same agreement.

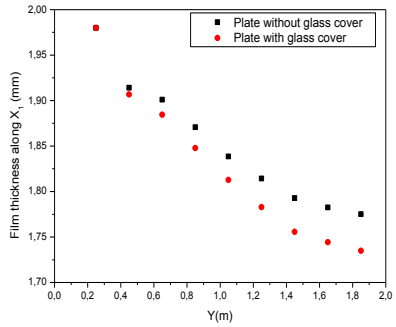

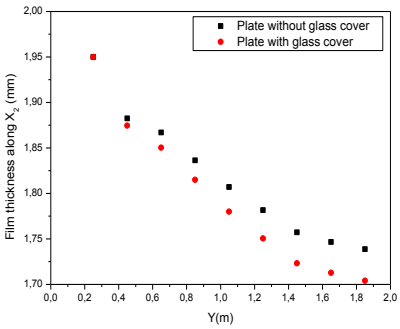

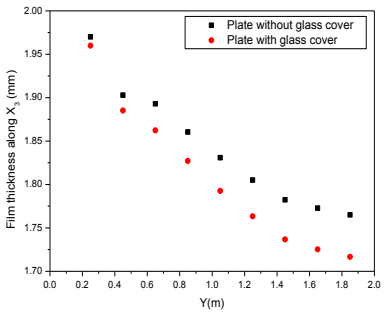

Fig. 9. The variation of film thickness

By solving (9), volume concentration is presented in fig.10. It increases along the plate. As the liquid evaporates, it water content decreases, so volume concentration increases. The initial volume concentration is about 0.0229%. At its release, its maximum concentration reached 0.0262% for X_2 when the plate is without glass cover. Comparing between covered and uncovered plate, volume concentration increases when plate has a glass cover. Its maximum is about 0.0274% along X_2.

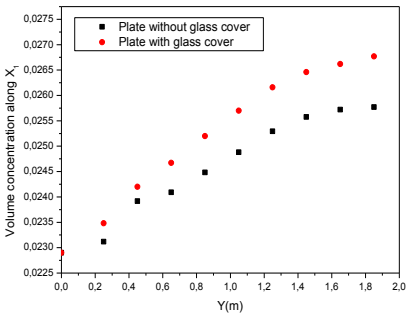

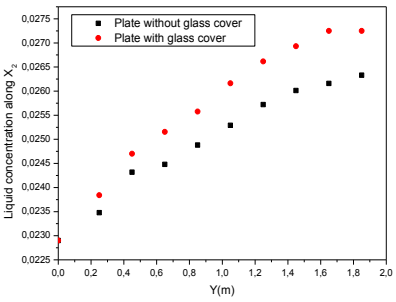

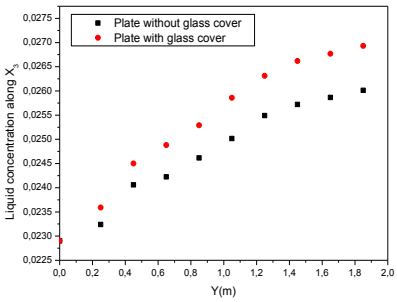

Fig. 10. Liquid concentration along the plate

Presented results concern an inlet liquid temperature of 40°C. Heat and mass balances are solved for different inlet liquid temperature. Comparing those results with experimental measurements, we obtain results presented in fig.11.

According to fig.11, when the inlet liquid temperature is about 19 and 30°C, the outlet liquid temperature is higher than the inlet. However, when the inlet liquid temperature is about 40 and 50°C, the outlet temperature is lower than the inlet one. This can be explained by the bottom of the plate where the liquid cooled and it temperature decreases. The offset between experimental and calculated results doesn't exceed 10%.

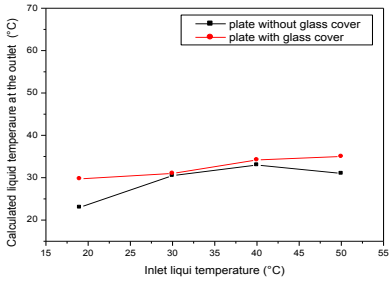

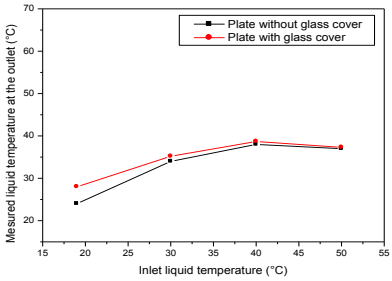

Fig. 11. Variation of the outlet temperature as function of the inlet one

When the inlet temperatures is between 19 and 40°C, the total evaporated flow rate increases if inlet temperature is increasing until stabilizing at 50°C. The maximum difference between measured and calculated results is acceptable.

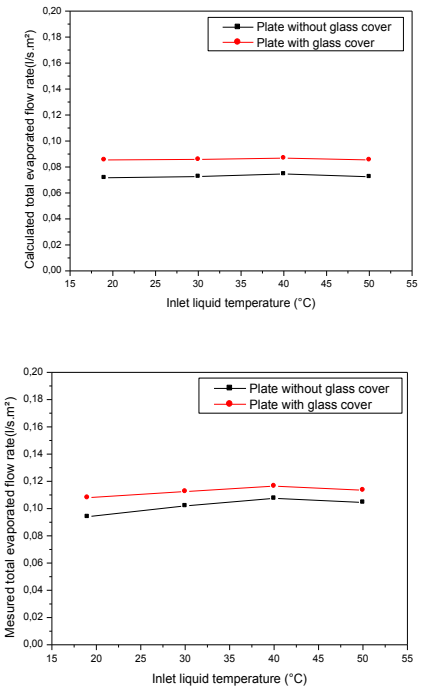

Fig.12. Variation of evaporated flow rate

Dufresne *et al.,* [27] is among the researchers who studied this phenomenon. He explained that the glass allows the solar radiation to pass while absorbing all of the infrared radiation. Thus, the glass absorbs the infrared radiation emitted by plate and is heated. As the glass temperature increases, it emits itself more infrared radiation; as a result, its temperature will increase until it loses as much energy as it receives. The radiation emitted by the glass is half emitted to the outside and lost, with the rest partly absorbed by the plate. Because the plate is now receiving more energy than it loses, its temperature will rise until it loses as much energy as it receives. This infrared radiation emitted by the extra plate is absorbed by the glass. These rays are transmitted several times until equilibrium is reached, wherein the plate temperature is higher than in the device without glass. As a result, the evaporated flow in better when the glass is used. This effect of the glass is the greenhouse effect. The purpose of the glass is to let radiation pass and inhibit the dissipation of the heat that forms between plate and glass under the influence of sunlight. The glass is used to limit the heat loss between the glass and the air and between the liquid and the air.

VI. Conclusion

A numerical and experimental study of evaporation of pig digestate after centrifugation was made. Firstly, a thermo-physical study has been done on the effluent which dry matter is about 2.3%. Three samples having different concentrations are prepared and characterized. This study shows that dynamic viscosity and heat capacity are strongly related to effluent concentration. In contrast to thermal conductivity, it depends on temperature not on liquid concentration.

Evaporation process was established when this liquid effluent flows on a stainless steel plate having a tilt angle of 30°. The plate is on one hand directly exposed to solar simulator radiations. On the other hand, the glass cover was removed.

A comparison between calculated and measured results was presented for two cases. In the first case, the inclined plate is directly exposed to solar simulator. In the second case, the plate has a glass cover. The plate temperature is higher when the plate is used with a glass cover, than its temperature when the plate is used without the glass cover.

The liquid is injected and its temperature is related to plate temperature. Thereby evaporated flow is proportional to film temperature; it would be better when the plate is used with the glass cover because the glass reduces heat losses due to convection.

The variation of evaporated flow rate is strongly related to plate and liquid temperature. The film thickness is affected by evaporated flow rate. The final volume concentration of effluent is about 0.0274%. The liquid has lost nearly 20% of its initial volume.

This study will be useful to have a better idea on liquid effluent recovery. This device will be designed on the roof of farms.

Acknowledgments

This work was carried out in the framework of a collaboration between the laboratory of automatic, mechanic and industrial and human computing (LAMIH) of The University of Valenciennes and Hainaut Cambresis and the laboratory of energetic and thermal and mass transfer (LETTM) of Sciences Faculty of Tunis, University Tunis El Manar. It's financially supported by the LAMIH laboratory. It's a part of PhD study.

References

[1] Aybar HS, Egelioglu F, Atikol U. An experimental study on an inclined solar distillation system. Desalination 2005; 180:285–9.
[2] Uwe Thiele, Edgar Knobloch, 2004. Thin liquid films on a slightly inclined heated plate. Physica D 190 (2004) 213–248.
[3] Jingchun Min, Yicun Tang, 2015. Theoretical analysis of water film evaporation characteristics on an adiabatic solid wall. International journal of refrigeration 53 (2015) 55e61.
[4] S.A. El-Agouz, Y.A.F. El-Samadony, A.E. Kabeel, 2015. Performance evaluation of a continuous flow inclined solar still. Desalination system Energy Conversion and Management 101 (2015) 606–615.
[5] Srithar, K. Mani, A. Comparison between simulated and experimental performance of an open solar flat plate collector for treating tannery effluent. International Communication in Heat and Mass Transfer 30 (4), 505-514 (2003).
[6] A. Leonard, S. Blacher, P. Marchot, M. Crine. Use of x-ray microtomography to follow the convective heat drying of wastewater sludges. Drying Technology 20 (4&5), 1053–1069 (2006).
[7] E. Mezaache a, M. Daguenet, 2005. Effects of inlet conditions on film evaporation along an inclined plate. Solar Energy 78 (2005)

535–542.
[8] Aybar HS. Mathematical modeling of an inclined solar water distillation system. Desalination 2006; 190:63–70.
[9] Agboola OP, Egelioglu F. Empirical investigations of two designs of incline solar water desalination system. Poland J Chem Technol 2012; 14:35–40.
[10] El-Agouz SA. Experimental investigation of stepped solar still with continuous water circulation. Energy Convers Manage 2014; 86:186–93.
[11] Raimundo, A.M., Gaspar, A.R., Oliveira, A.V.M., Quintela, D.A., 2014. Wind tunnel measurements and numerical simulations of water evaporation in forced convection airflow. Int. J. Therm. Sci. 86, 28e40.
[12] Yang, X., Yan, Y.Y. Molecular dynamics simulation for microscope insight of water evaporation on a heated magnesium surface. Appl. Therm. Eng. 31, 640e648 (2011).
[13] Yu, J.P., Wang, H. A molecular dynamics investigation on evaporation of thin liquid films. Int. J. Heat Mass Transf. 55, 1218e1225 (2012).
[14] Leu, J.S., Jang, J.Y., Chou, Y. Heat and mass transfer for liquid film evaporation along a vertical plate covered with a thin porous layer. Int. J. Heat. Mass Transf. (2006) 49, 1937e1945.
[15] Brau. J. Support de cours de convection pour 3 GCU. Insa de Lyon, department de Génie Civil et Urbanisme (2006).
[16] Srithar K, Mani A. Open fibre reinforced plastic (FRP) flat plate collector (FPC) and spray network systems for augmenting the evaporation rate of tannery effluent (soak liquor). Solar Energy 81 (2007) 1492–1500.
[17] Chen T.S, Tien J.P, Armaly B.F. Natural convection on horizontal, inclined and vertical plates with variable surface temperature or heat flux. Int. J. Heat. Mass. Transfer. Vol. 29, n°10, p1465-78 (1986).
[18] Huetz-Aubert, J. F. Sacadura. Mesure des émissivités et des réflectivités monochromatiques directionnelles des matériaux opaques. Revue Phys. Appl. 17, p251 – 260 (1981).
[19] Huetz J, Petit JP. Notion de transfert thermique par convection. Technique de l'ingénieur, traité Génie énergétique (1986).
[20] Bouchekima B, Gros B, Ouahes R, Diboun M. Brakish water desalination with heat recovery. Desalination 138 p147 – 155 (2001).
[21] Bouchekima B, Gros B, Ouahes R, Dibouna M. The performance of the capillary film solar still installed in South Algeria. Desalination 137 (2001) 31-38.
[22] Kumar R, Rosen M.A. Thermal performance of investigated collector storage solar water heater with corrugated absorber surface. Applied Thermal Engineering 30(2010)1764e1768.
[23] Chaker A, Menguy G. Efficacité Interne d'un Distillateur Solaire Sphérique. Rev. Energ. Ren. Journées de Thermique (2001) 53-58.
[24] Suneja S, Tiwari G.N. Effect of water flow on internal heat transfer solar distillation. Energy Conversion & Management 40 (1999) 509±518.
[25] Kannan R, Selvaganesan C, Vignesh M, Ramesh Babu B, Fuentes M, Vivar M, Skryabin I, Srithar K. Solar still with vapor adsorption basin: Performance analysis. Renewable Energy 62 (2014) 258-264.
[26] Ben Jabrallah S, Cherif A.S, Dhifaoui B, Belguith A, Corriou JP. Experimental study of the evaporation of a falling film in a closed cavity. Desalination 180(2005) 197-206.
[27] Dufresne J. L, C. Youinou, 2007. Cent réponses sur le réchauffement de la planète, Tournon, (2007), 120 p.